minimum at the waveguide width w ~150-200 nm, while the propagation length stabilizes in the region of ~5 μm, corresponding to ten SPP wavelengths. Here we note an interesting fact, in contrast with the tendencies described above; for wide waveguides the mode area and the propagation length decrease as the waveguide height changes from 300 nm (where it is close to the one at a planar Si/Al interface L_{prop} ≈7.8 μm) to 150 nm [Figs. 2(b) and 2(c)]. This corresponds to the pattern for wide waveguides when the top polymer/air interface effectively push the fields into the metal, which then leads to the decrease of the mode area [Fig. 2(c)] and increase of losses due to the increased field confinement near the metal [Fig. 2(b)]. This remains correct up to waveguide height of several tens of nanometres.

The mode effective area was estimated using two approaches. In the first one, we carefully mapped the absolute value of power flow along the waveguide $|P_z|$ and found the area S_{eff}^{A} inside the constant level contour, encircling (1-3e^{-2}) part of the total $|P_z|$ integral [Fig. 2(c)]. This corresponds to the part of the intensity encircled by 1/e field decay contour in the case of the Gaussian distribution. We used an integral rather than a magnitude condition for the level defining the contour, because with various waveguide cross-sections, various mode decay dependencies should be expected. In this case the integral condition for the contour is more appropriate. The second approach we used is based on well known formula for mode area estimation $S_{eff}^{B} = \left(\int IdS\right)^2 \Big/ \int I^2 dS$, where I is the field intensity. The results for S_{eff}^{B} are presented in the inset to Fig. 2(c). Both approaches return very similar dependencies. To understand the trade-off between the mode confinement and propagation length, we introduced a figure of merit (FOM) $M_1 = 2\sqrt{\pi} \cdot L_{prop} \Big/ \sqrt{S_{eff}^{A}}$, defined in a way similar to Ref. 17. Generally, for all the waveguide heights, M_1 is a monotonically decreasing function of the waveguide width [Fig. 2(d)]. However, for small waveguide widths, the large effective mode area and the effective mode index close to the refractive index of the surrounding media are hardly compatible with the requirements of high-density photonic integration and result in strong losses at sharp waveguide bends.

4. Figures of merit

The figure of merit M_1 provides an easy and quick outlook of the waveguide performance. However, to gain insight into the performance of the waveguides in terms of switching and modulation applications and achievable density of photonic integration, we have introduced modified FOMs. The square root of the mode area in the denominator of M_1 is effectively a measure of how closely parallel waveguides can be packed on a chip. However, modes with the same effective areas can be coupled more efficiently or less efficiently to the neighboring waveguide depending on their spatial field distributions. Therefore, the figure of merit was modified in order to represent the coupling efficiency directly. When two parallel waveguides are placed next to each other, the coupling leads to the tunneling of the mode from one waveguide to another with a full energy transfer after a distance L_{coupl} [10]. As a criterion for cross-talk estimations, L_{coupl} = 250 μm was chosen for all waveguide cross-sections based on a typical propagation length for Si-SPP waveguides, so that after ~5 propagation lengths less than 1% of the energy will be coupled to the neighboring waveguide, which can be neglected. For each cross-section the waveguide centre-to-centre separation, d, satisfying this condition was found. In order to do this, an eigenmode problem is solved for the two coupled waveguides, and L_{coupl} is then determined as half a period of beating between symmetric and asymmetric modes in the system $L_{coupl} = \lambda \Big/ \left[2\left(n_{eff}^{sym} - n_{eff}^{asym}\right)\right]$. As a result, the first modification of the figure of merit $M_A = L_{prop} \Big/ d$ is obtained [Fig. 3(a)]. The general trends here are the same as for M_1, diverging from this behaviour as M_A starts to increase for wider waveguides. It can be explained by a faster decrease of the exponential tail in the horizontal direction than predicted by the average mode area estimation approach used in M_1. This leads to possible separation distances of the order of 10 nm for waveguides wider than ~350 nm.

#125663 - $15.00 USD Received 18 Mar 2010; revised 23 Apr 2010; accepted 5 May 2010; published 19 May 2010

Such separations are rather unrealistic from a fabrication point of view, and we introduced a minimum separation between the waveguides of 100 nm. This constraint is responsible for an abrupt change in the trends in the graphs at larger the waveguide widths.

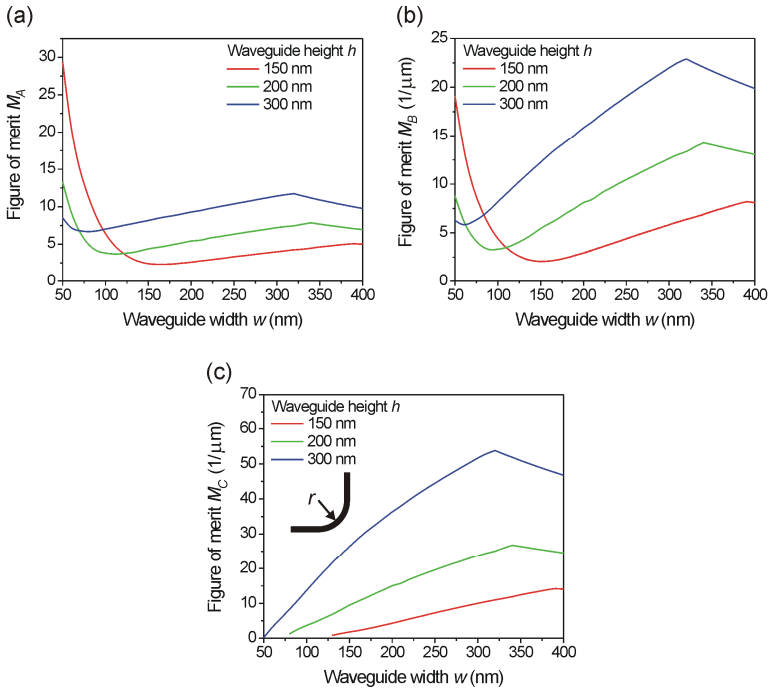

Fig. 3. Figures of merit for Si/Al SPP waveguide defined for monitoring performance with respect to (a) waveguide separation, M_A and (b) MZI and WRR functionalities, M_B. (c) M_C combines M_A, M_B, and bend radius performance. Please see the text for details.

Considering the performance of waveguide circuitry elements such as Mach-Zehnder interferometers (MZIs) and waveguide ring resonators (WRRs), it becomes apparent that not absolute L_{prop} but the mode propagation length expressed in terms of the mode wavelength $L_{prop}/(\lambda/n_{eff})$ is now the important parameter since it governs the phase-related effects achievable during the mode propagation. Following this considerations, the figure of merit is modified to be $M_B = L_{prop} n_{eff}/\lambda d$ [Fig. 3(b)]. In terms of density of integration and phase-related functionalities, due to the high effective mode indexes, waveguides having larger cross-sections compete with waveguides having smaller cross-sections but larger SPP propagation lengths: the figure of merit M_B for a 300 × 300 nm^2 waveguide is approximately the same as for a 50 × 150 nm^2 waveguide.

A crucial parameter for the realization of a multi-branched waveguide circuitry is the radius with which it is possible to bend the waveguide, while still having acceptable radiation losses [see an inset to Fig. 3(c)]. This parameter defines the size of all waveguide elements, such as splitters, WRRs, MZIs, etc. The ideal waveguide radius is a trade-off between Ohmic losses (higher for bigger radii) and radiation losses (higher for smaller radii). To determine this radius for each waveguide cross-section a set of 3D propagation-mode numerical simulations has been performed and used to define an all-inclusive figure of merit $M_C = L_{prop} n_{eff}/\lambda d \cdot T/(r/\lambda) = L_{prop} n_{eff}/d \cdot T/r$, where r is the ideal bending radius and T is the corresponding bend transmission. Due to lower values of n_{eff}, waveguides with smaller cross-sections have a low refractive index contrast with the surrounding media. This leads to large radiation losses and consequently large possible bending radii, of the order of several micrometres. Therefore, the behavior of the figure of merit for them is dramatically changed

#125663 - $15.00 USD Received 18 Mar 2010; revised 23 Apr 2010; accepted 5 May 2010; published 19 May 2010

[Fig. 3(c)], with M_C tending to zero. On the other hand, waveguides with larger cross-sections allow bending radii smaller than a micron (for example for a 300 × 300 nm^2 waveguide, the ideal bending radius is r = 0.5 μm). For these waveguides the figure of merit is relatively increased. It should finally be noted that the choice of figure of merit and in particular the weighting factors for its various parameters should be defined by the specific application in mind, e.g., if strong mode confinement is required, it is not necessarily the case that a long propagation length is needed. Thus, if one of the parameters included in the FOM is significantly larger for one of the waveguides, this may completely hide the advantages of another waveguide in terms of a different parameter (c.f. mode area and propagation length).

5. Practical implementation in nanophotonic circuits: materials, GVD and gain

In order to compare various metallic material platforms for Si-based DLSPPWs the waveguide guiding properties have been studied for the case of Au, Al, and Cu. The dielectric constants for simulations were taken from Ref. 16, where there are two sets of values for Au and Al depending on different sample preparation and measurement techniques employed in the source references. From Fig. 4 we can conclude that copper is inferior to gold and aluminum in terms of plasmonic properties. Although it provides the highest effective refractive index and the smallest mode area, high Ohmic losses significantly reduce the figure of merit. On the other hand, for the wide range of waveguide cross-sections, the plasmonic properties of aluminum are very similar to those of gold. This makes it a promising candidate for the metallic component of Si-based SPP waveguide circuitry.

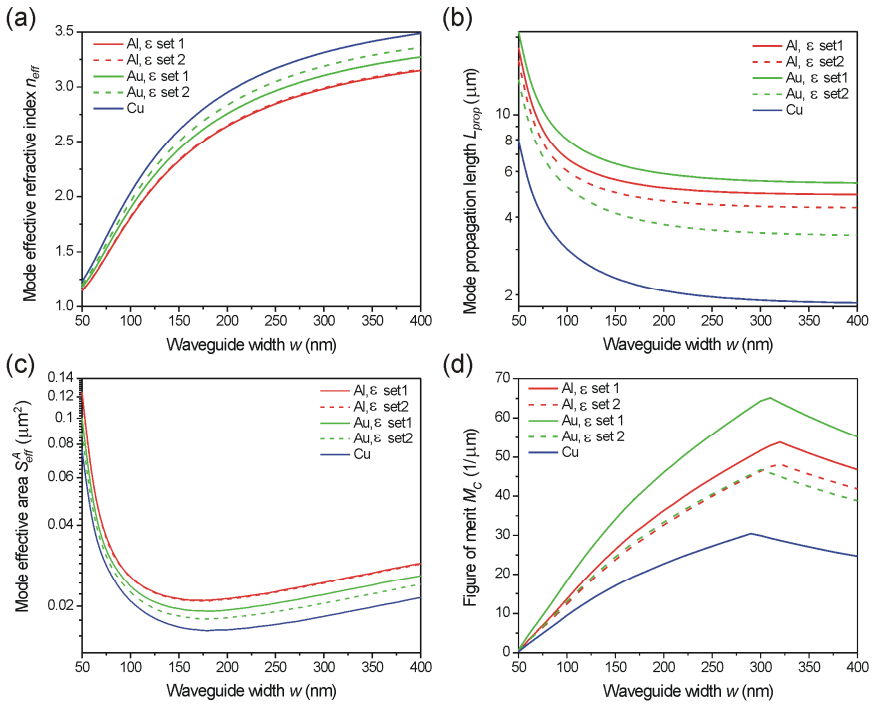

Fig. 4. (a) Effective refractive index, (b) propagation length, (c) effective mode area, and (d) figure of merit M_C for Si-SPP waveguide with height h = 300 nm as a function of its width w for various metals: Au, Al and Cu.

Since both Si and metal materials are highly dispersive, and the waveguide dispersion essentially depends on geometrical factors, it is important to estimate the Si-based DLSPPW performance for transmitting short pulses. Broadening of the pulse during its propagation is defined by a group velocity dispersion (GVD) parameter $\beta_2 = \partial^2 k_{SPP} / \partial \omega^2$, which is

#125663 - $15.00 USD Received 18 Mar 2010; revised 23 Apr 2010; accepted 5 May 2010; published 19 May 2010

presented for the case of a 100 × 300 nm^2 Si/Al waveguide in the inset to Fig. 1(b). Near telecommunication wavelength of 1550 nm (0.8 eV), β_2 passes zero ensuring a good waveguide performance. The dispersion length for 100 fs pulses is on average 1 mm, which is far beyond the length scale at which these types of waveguide are required. Even at a bit rate of 10 Tb/s, after 5 mode propagation lengths (34 μm) broadening of the pulse is only ~1%. Thus, these waveguides are not dispersion limited. Moreover, the zero-dispersion point is situated at the datacom frequency range [Fig. 1 (b), insert] so that GVD can be further reduced by tuning waveguide geometrical parameters.

For practical implementation in nanophotonic circuits, the Si-based SPP waveguide should be covered with another material, for example silica or polymer. In contradiction with a usual tendency, the propagation length of the mode can be actually increased by coating with material having n = 1.45 (from 6.74 μm to 7.57 μm for a 100 × 300 nm^2 waveguide, remains almost unchanged for a 300 × 300 nm^2 waveguide). At the same time, the refractive index contrast decreases from 1.81/1 to 2.03/1.45 for a 100 × 300 nm^2 waveguide and from 2.98/1 to 3.01/1.45 for a 300 × 300 nm^2 waveguide. In the latter case, the decrease is less dramatic and essentially should not lead to an increase of the waveguide bending radius.

Now we consider the case of coating in connection with possible amplification of the SPP mode propagating in the waveguide. There are two options to introduce the gain medium: using the waveguide core or, alternatively, the waveguide surroundings. The choice of the most efficient approach depends on the waveguide cross-section. For 100 × 300 nm^2 waveguide, the gain in the core required for lossless propagation of the mode corresponds to $\mathrm{Im}\left(\varepsilon_{Si}^{*}\right) = 0.14i$, while for active surroundings to $\mathrm{Im}\left(\varepsilon_{silica}^{*}\right) = 0.03i$. This corresponds to modal gain values of ~1620 cm^{-1} and ~850 cm^{-1}, respectively. Taking into account that the gain coefficient is proportional to the refractive index of the host medium [18], it can be concluded that the density of active centers (e.g., quantum dots or lasing atoms) required for lossless mode propagation for both options is approximately the same. This should be expected since the energy distribution between the core and the coating is approximately equal. For a 300 × 300 nm^2 waveguide the situation is different. Most of the mode energy (~90%) is located in the core of the waveguide, so the active coating requires high gain values of ~$2.3 \cdot 10^4$ cm^{-1}. On the other hand, the gain required in the amplifying core is similar (~1640 cm^{-1}) to that for the previous cross-section.

6. Conclusion

In conclusion, we have numerically demonstrated efficient singlemode Si-based plasmonic waveguides. The high refractive index of silicon leads to deep subwavelength localization of the photonic signal, higher than in conventional Si-based waveguides, and moreover, to the possibility of sharp (down to 500 nm radius at telecom wavelengths) waveguide bending, important for photonic integration. While the absolute propagation length of the mode is inferior to one in conventional Si-waveguides, for the design of the photonic circuits it is extremely important how strongly the signal is confined within the waveguide and can be affected during propagation by external stimuli. Si-loaded plasmonic waveguides provide unrivalled advantages and are simpler to integrate in CMOS technology than other types of plasmonic waveguide with comparable figures of merit. The M_1 figure of merit is the same for Si-loaded SPP waveguides and plasmonic slot waveguides, it is approximately 2 and 3 times smaller than for long-range plasmon waveguides and polymer-based DLSPP waveguides, respectively, because of the larger propagation length (while also larger mode area) in the latter cases. An Al/Si material platform ensures good mode propagation parameters and is compatible with CMOS fabrication technology. It is possible, theoretically, to use separations between the waveguides as small as a few tens of nanometres.

To compare waveguide performance in various applications, a set of figures of merits have been developed providing for simple comparisons between both passive and active functionalities. Introduction of gain for achieving lossless SPP propagation is also possible either within the core or surrounding of the proposed guides. We have demonstrated the

#125663 - $15.00 USD Received 18 Mar 2010; revised 23 Apr 2010; accepted 5 May 2010; published 19 May 2010

potential for on-chip data transfer at rates up to 10 Tb/s, which can be further improved by design of the appropriate waveguide geometry.

Finally, high-refractive index DLSPP waveguides can be combined with nonlinear and electro-optical effects. For example, $BaTiO_3$ thin films possess both high refractive index n = 2.3 and a large electro-optic (~100 pm/V) and nonlinear optical coefficients. Therefore, $BaTiO_3$-based SPP waveguides provide a similar level of photonic integration as discussed above for Si-loaded SPP waveguides and can be used for realization of SPP active components, taking advantage of the plasmonic field enhancement.

Acknowledgements

This work was support by EPSRC (UK) and EC FP6 STREP PLASMOCOM. The authors acknowledge the fruitful discussions with S. I. Bozhevolnyi and W. Dickson.

#125663 - $15.00 USD Received 18 Mar 2010; revised 23 Apr 2010; accepted 5 May 2010; published 19 May 2010